

Three Steps to Chaos—Part I: Evolution

Michael Peter Kennedy

Abstract—Linear system theory provides an inadequate characterization of sustained oscillation in nature. In this two-part exposition of oscillation in piecewise-linear dynamical systems, we guide the reader from linear concepts and simple harmonic motion to nonlinear concepts and chaos. By means of three worked examples, we bridge the gap from the familiar parallel RLC network to exotic nonlinear dynamical phenomena in Chua's circuit. Our goal is to stimulate the reader to think deeply about the fundamental nature of oscillation and to develop intuition into the chaos-producing mechanisms of nonlinear dynamics.

In order to exhibit chaos, an autonomous circuit consisting of resistors, capacitors, and inductors must contain

- i) at least one nonlinear element
- ii) at least one locally active resistor
- iii) at least three energy-storage elements.

Chua's circuit is the simplest electronic circuit that satisfies these criteria. In addition, this remarkable circuit is the *only* physical system for which the presence of chaos has been proven mathematically. The circuit is readily constructed at low cost using standard electronic components and exhibits a rich variety of bifurcations and chaos.

In Part I of this two-part paper, we plot the evolution of our understanding of oscillation from linear concepts and the parallel RLC resonant circuit to piecewise-linear circuits and Chua's circuit. We illustrate by theory, simulation, and laboratory experiment the concepts of equilibria, stability, local and global behavior, bifurcations, and steady-state solutions. In Part II, we study bifurcations and chaos in a robust practical implementation of Chua's circuit.

I. MOTIVATION

DESPITE THE FACT that many common phenomena observed daily in circuits and signal processing systems can be explained *only* in terms of nonlinear models, the study of nonlinear dynamics is still a great uncharted territory in systems analysis. The common rule in engineering education has been "linearize; then analyze." With such a deep-rooted philosophy, it comes as a great surprise to many practicing engineers when the linear concepts long-since engrained in their minds are unable to account for experimentally observed phenomena.

Throughout the history of science, complex nonlinear phenomena have been noticed by experimentalists but, more often than not, have been disregarded because the concepts for explaining them simply did not exist. A classic example of this is the driven neon bulb oscillator circuit examined by the eminent Dutch electrical engineer and physicist van der Pol. He reported his oscillator experiment in *Nature* magazine in 1927 [1], noting that "often an irregular noise is heard"

Manuscript received April 1, 1993; revised June 5, 1993. This paper was recommended by Guest Editor L. Chua.

The author is with the Department of Electronic and Electrical Engineering, University College Dublin, Dublin, Ireland.
IEEE Log Number 9211603.

in the circuit. He dismissed this "noise" as "a subsidiary phenomenon" not worthy of further investigation. It is only in more recent times that the conditions under which such noise is generated are becoming understood [2]. A new vocabulary of nonlinear science has emerged as we begin to grapple with a variety of unusual but ubiquitous and robust dynamical behaviors; this is the language of attractors, bifurcations, and chaos [3], [4].

It is important that we should understand the ideas of nonlinear dynamics at a deep level so that no naturally occurring phenomenon can be considered strange. Even in this field, the steady-state behavior of a chaotic system has been termed a "strange" attractor [3], [5]. We now know that such attractors are not at all strange or unusual but pervade throughout the natural and physical world. Complicated waveforms that are characteristic of strange attractors and so often mistaken for experimental noise commonly occur in digital filters [6], phase-locked loops [7], and synchronization circuits [8].

By virtue of their complexity, exotic nonlinear behaviors such as these have stubbornly refused to yield to the simple analysis we apply to linear systems. In stark contrast to linear systems, it is not possible to obtain explicit solutions for most nonlinear systems. Nevertheless, there is "order" and "universality" in large classes of nonlinear phenomena that make them ideally suited to *qualitative* analysis. Many complex systems, although multidimensional, exhibit behavior that can be described by models of low order. In particular, the nonlinear dynamics of high-dimensional circuits can often be understood by examining their projections onto 2-D planes. These lower order models are often adequate to describe the behavior of the system. One such technique (the 2-D Hopf bifurcation theorem [9]) can be used successfully to predict the onset of oscillation in systems of higher order.

For example, the microwave oscillator designer seldom takes account of every parasitic capacitance and inductance when developing a circuit. Implicit in her design methodology is an understanding that the steady-state output of the circuit is similar to that of a lower dimensional circuit. It is only when the predictions of the lower dimensional model fail to match experimental observations that more "parasitic" elements are added to the model.

It is very important, therefore, to investigate these low-order systems completely with a view to classifying behaviors and simplifying models of higher order systems. It is for precisely this reason that the RLC resonant circuit is the established paradigm for understanding simple linear oscillatory behavior. With the great advances in nonlinear circuit theory over the past 30 years (see, for example, [10]–[12]), it is now possible to explain highly complex nonlinear behaviors

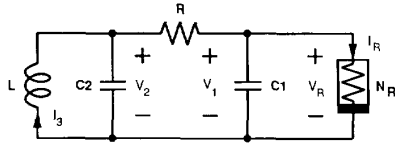


Fig. 1. Chua's circuit consists of a linear inductor L , two linear capacitors (C_2, C_1), a linear resistor R , and a voltage-controlled nonlinear resistor N_R .

with simple models and minor extensions to linear circuit theory.

One of the simplest and most widely studied real *nonlinear* dynamical systems is Chua's circuit [13], which is shown in Fig. 1. This consists of a linear inductor L , a linear resistor R , two linear capacitors C_1 and C_2 , and a single voltage-controlled¹ nonlinear resistor N_R called a *Chua diode* [14]. This remarkable circuit is the *only* physical system for which the presence of chaos (in the sense of Shilnikov) has been established experimentally, confirmed numerically, and proven mathematically [13]. The circuit is readily constructed at low cost using standard electronic components [14] and exhibits a rich variety of bifurcations and chaos [15].

Just as the parallel RLC circuit is the system of lowest order that can model the onset of oscillation in a dynamical system, so Chua's circuit is the system of lowest order that can capture the rich *nonperiodic* dynamics of higher order systems.

II. OUTLINE

In this tutorial paper, we venture into the exciting world of nonlinear dynamics. With elementary linear and piecewise-linear circuit theory, we guide the reader in three steps from sinusoidal oscillation in a linear RLC circuit to chaos in Chua's circuit. By means of background theory and worked examples, we study the concepts of steady-state solutions, equilibrium points, stability, bifurcations, limit cycles, and chaos.

In Part I, we review some basic ideas in dynamical systems theory using the linear parallel RLC resonant circuit as our example. We illustrate the concepts by means of theory, simulation, and laboratory experiment.

We introduce piecewise-linear circuit theory as a logical and trivial extension of linear circuit theory that enables us to study simple nonlinear concepts. Building on this solid theoretical foundation, we show how the parallel linear RLC resonant circuit (the simplest paradigm for understanding *periodic* steady-state phenomena in linear circuits) evolves through two second-order piecewise-linear circuits into Chua's circuit (the simplest paradigm for studying *nonperiodic* phenomena in nonlinear circuits).

In Part II, we concentrate on Chua's oscillator. Using the piecewise-linear circuit theory introduced in Part I, we focus our attention on third-order dynamics. By means of theory, computer simulation, and laboratory experiment, we describe in detail the geometric structure, bifurcations, and periodic and nonperiodic oscillatory phenomena in Chua's circuit. We begin with the classic linear parallel RLC circuit.

¹ A two-terminal nonlinear resistor is called *voltage-controlled* if the current into its terminals may be written as a function of the voltage across it.

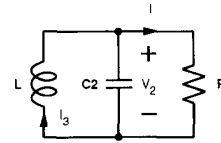


Fig. 2. Linear parallel RLC resonant circuit

III. THE LINEAR RLC CIRCUIT IS A POOR MODEL OF REALITY

Consider the familiar parallel-tuned RLC resonant circuit shown in Fig. 2. This consists of two linear, lossless, passive, *energy-storage* elements (a linear inductor L and a linear capacitor C_2) and a linear resistor R with conductance $G = 1/R$. We assume throughout this paper that L and C_2 are both *positive*.

In this section, we use this circuit to illustrate elementary concepts in dynamical systems theory. We show that although the circuit is a useful framework in which to introduce ideas of stability and oscillation, its linear nature restricts its usefulness. In particular, we explain why the linear RLC circuit is a poor model of sustained oscillation in nature and use this argument to motivate the introduction of piecewise-linear circuit theory. We begin with a qualitative physical description of the behavior of the model.

3.1. Qualitative Description

Assume that the current in the inductor at time $t = 0$ is I_{30} and that the capacitor is initially charged to a voltage V_{20} . The total *energy* stored in the magnetic field of the inductor, and the electric field of the capacitor is thus $\frac{1}{2}LI_{30}^2 + \frac{1}{2}C_2V_{20}^2$ [16]. What happens for $t > 0$? There are three cases to consider:

If G is positive, the resistor is said to be *dissipative*. The energy initially stored in the capacitor and inductor is dissipated as heat in the resistor as the magnetic and electric fields collapse. $V_2(t)$ and $I_3(t)$ approach zero either *monotonically* (in which case we call the response *overdamped*) or in the form of exponentially decaying sinusoids (*underdamped*) as shown in Fig. 3(a).

If G is negative, the resistor has *negative dissipation*; it *supplies* energy to the rest of the circuit. In this case, the energy stored in the circuit *increases* with time: $V_2(t)$ and $I_3(t)$ have exponentially growing envelopes. This is illustrated in Fig. 3(b).

If G is identically equal to zero (corresponding to an *open circuit*), the circuit is said to be *undamped*. The energy that was initially stored in the capacitor and inductor cannot be dissipated (there are no resistive losses) but simply oscillates back and forth between these two elements. The voltage and current waveforms $V_2(t)$ and $I_3(t)$ are *sinusoidal*. In the absence of damping, this sinusoidal oscillation continues indefinitely; the circuit is then called a *harmonic oscillator*. Typical voltage and current waveforms for the harmonic oscillator are shown in Fig. 3(c).

To obtain a quantitative description of this circuit, we first develop a mathematical formulation of the problem. As electrical engineers, circuit theory provides us with a modeling framework for analyzing the behavior of physical systems.

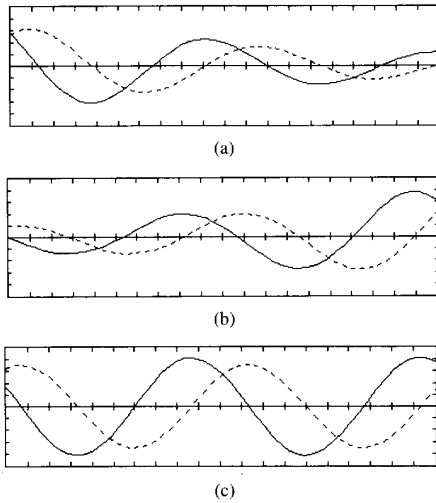


Fig. 3. Typical voltage and current waveforms for the linear parallel RLC circuit shown in Fig. 2 with $L = 18\text{mH}$ and $C_2 = 100\text{nF}$: (a) $G = 500\mu\text{S}$ (positive damping, underdamped); (b) $G = -500\mu\text{S}$ (negative damping, underdamped); (c) $G = 0$ (undamped). Horizontal axis: time, $25\mu\text{s}/\text{div}$; vertical axis: I_3 (dashed line), $200\mu\text{A}/\text{div}$, V_2 (solid line), $100\text{mV}/\text{div}$.

3.2. Quantitative Description

State Equations, Vector Fields, and Trajectories: A lumped² circuit containing resistive elements (resistors and voltage and current sources) and n energy-storage elements (capacitors and/or inductors) can be described by a system of ordinary differential equations of the form:

$$\dot{\mathbf{X}}(t) = \mathbf{F}(\mathbf{X}(t), t), \mathbf{X}(0) = \mathbf{X}_0$$

where $\mathbf{X}(t) = (X_1(t), X_2(t), \dots, X_n(t))^T \in \mathbb{R}^n$ is called the *state vector* and $\mathbf{F}(\mathbf{X}(t), t) = (F_1(\mathbf{X}(t), t), F_2(\mathbf{X}(t), t), \dots, F_n(\mathbf{X}(t), t))^T$ is an n -dimensional map $\mathbf{F} : \mathbb{R}^n \times \mathbb{R}^+ \rightarrow \mathbb{R}^n$. \mathbf{X}_0 is the *initial condition*, and $\dot{\mathbf{X}}(t)$ denotes the derivative of $\mathbf{X}(t)$ with respect to time. This is called the *initial value problem* [17], and a solution $\mathbf{X}(t)$ is called a *trajectory*.

In the nonlinear dynamics literature, $\mathbf{F}(\mathbf{X}(t), t)$ is called a *vector field* because it defines the *direction* and *speed* of a trajectory at every point in the state space and at every instant of time. If the vector field depends only on the state and is *independent* of time t , then the system is said to be *autonomous* and may be written as

$$\dot{\mathbf{X}}(t) = \mathbf{F}(\mathbf{X}(t)), \mathbf{X}(0) = \mathbf{X}_0$$

or simply

$$\dot{\mathbf{X}} = \mathbf{F}(\mathbf{X}), \mathbf{X}(0) = \mathbf{X}_0. \quad (1)$$

Each of the circuits that we study in this paper is *autonomous*.

By definition, the vector field of an autonomous circuit is a *function* and is therefore unique at every point \mathbf{X} in the state space. An important consequence of this is that a trajectory of the system cannot go through the same point twice in two

²A *lumped* circuit is one whose physical dimensions are small compared to the wavelengths of its voltage and current waveforms [16].

different directions. In particular, trajectories of a 2-D system *cannot cross each other*; this has important implications for the possible solutions of two-dimensional systems.

The parallel RLC circuit of Fig. 2 is characterized by a pair of ordinary differential equations and an initial state. Choosing V_2 and I_L as *state variables*, we write the *state equations*

$$\frac{dI_3}{dt} = -\frac{1}{L}V_2 \quad (2)$$

$$\begin{aligned} \frac{dV_2}{dt} &= \frac{1}{C_2}I_3 - \frac{1}{C_2}I \\ &= \frac{1}{C_2}I_3 - \frac{G}{C_2}V_2 \end{aligned} \quad (3)$$

with $I_3(0) = I_{30}$ and $V_2(0) = V_{20}$.

We illustrate the vector field by drawing vectors at uniformly spaced points in the 2-D state space defined by (I_3, V_2) . Starting from a given initial condition (I_{30}, V_{20}) , the solution of the differential equation is the locus of points plotted out by the state as it moves through the vector field following the direction of the arrow at every point. Fig. 4 shows typical vector fields and trajectories of the circuit.

Equilibrium Point(s): An *equilibrium point* of (1) is a state \mathbf{X}_Q at which the vector field is zero. Thus, $\mathbf{F}(\mathbf{X}_Q) = 0$ and $\mathbf{X}_Q(t) = \mathbf{X}_Q$; a trajectory starting from an equilibrium point remains indefinitely at that point. An equilibrium point of an electronic circuit is simply a *dc solution*.

Turning to our linear RLC resonant circuit once more and solving for the equilibrium points of (2) and (3), we find just one solution $(I_{3Q}, V_{2Q}) = (0, 0)$. This corresponds to the zero-energy state of the circuit.

Linear and Affine Systems: The vector field $\mathbf{F}(\mathbf{X})$ of an autonomous *linear* dynamical system has the special form $\mathbf{F}(\mathbf{X}) = \mathbf{A}\mathbf{X}$, where \mathbf{A} is called the *system matrix*. For a linear system, (1) takes the simpler form

$$\dot{\mathbf{X}} = \mathbf{A}\mathbf{X}, \mathbf{X}(0) = \mathbf{X}_0.$$

For example, the state equations of the linear parallel RLC circuit may be rewritten

$$\begin{bmatrix} \dot{I}_3 \\ \dot{V}_2 \end{bmatrix} = \begin{bmatrix} 0 & -\frac{1}{L} \\ \frac{1}{C_2} & -\frac{G}{C_2} \end{bmatrix} \begin{bmatrix} I_3 \\ V_2 \end{bmatrix}.$$

A vector field of a linear system is zero only at the origin so that the system has just one equilibrium point (as we have seen for our RLC circuit).

Closely related to a linear system and of particular interest for the analysis of piecewise-linear circuits is an *affine* system. An *affine* system is one that is described by

$$\dot{\mathbf{X}} = \mathbf{A}\mathbf{X} + \mathbf{b}, \mathbf{X}(0) = \mathbf{X}_0$$

where \mathbf{b} is a constant vector. Clearly, when $\mathbf{b} \equiv \mathbf{0}$, the system is *linear*.

If \mathbf{A}^{-1} exists, the equilibrium point \mathbf{X}_Q of an affine system is defined by

$$\mathbf{X}_Q = -\mathbf{A}^{-1}\mathbf{b}.$$

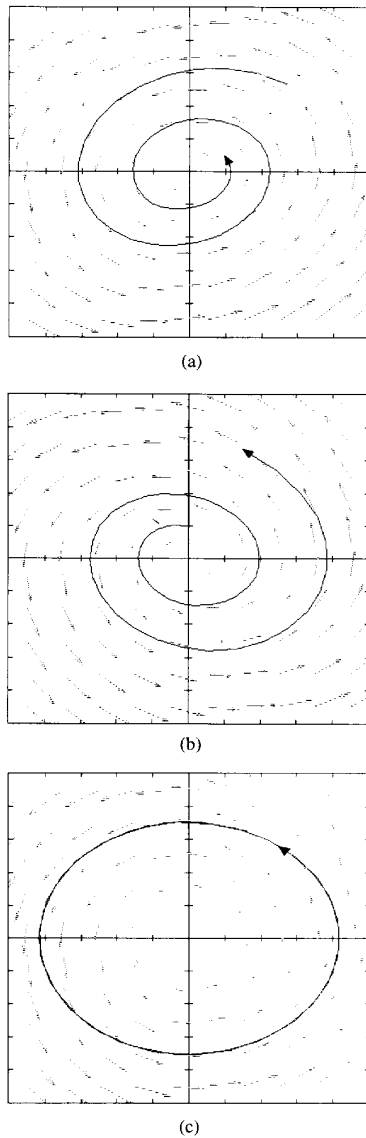


Fig. 4. Typical vector fields for the linear parallel RLC resonant circuit with $L = 18\text{mH}$ and $C_2 = 100\text{nF}$: (a) $G = 500\mu\text{S}$ (> 0); trajectories are pushed together as they spiral toward the origin; (b) $G = -500\mu\text{S}$ (< 0); trajectories are stretched apart as they spiral away from the origin; (c) $G = 0$; trajectories follow closed paths with an amplitude defined by the initial conditions. Horizontal axis: i_3 , $250\mu\text{A}/\text{div}$ vertical axis: v_2 , $100\text{mV}/\text{div}$.

Linearization: To analyze the behavior of a dynamical system in the neighborhood of a point \mathbf{X}_Q , we write $\mathbf{X} = \mathbf{X}_Q + \mathbf{x}$ and substitute into (1) to obtain

$$\begin{aligned} \dot{\mathbf{X}}_Q + \dot{\mathbf{x}} &= \mathbf{F}(\mathbf{X}_Q + \mathbf{x}) \\ &\approx \mathbf{F}(\mathbf{X}_Q) + \mathbf{J}_F(\mathbf{X}_Q)\mathbf{x} \end{aligned} \quad (4)$$

where we have kept just the first two terms of the Taylor series expansion of $\mathbf{F}(\mathbf{X})$ about \mathbf{X}_Q . The *Jacobian matrix* $\mathbf{J}_F(\mathbf{X})$ is

the matrix of partial derivatives of $\mathbf{F}(\mathbf{X})$:

$$\mathbf{J}_F(\mathbf{X}) = \begin{bmatrix} \frac{\partial F_1(\mathbf{X})}{\partial X_1} & \frac{\partial F_1(\mathbf{X})}{\partial X_2} & \cdots & \frac{\partial F_1(\mathbf{X})}{\partial X_n} \\ \frac{\partial F_2(\mathbf{X})}{\partial X_1} & \frac{\partial F_2(\mathbf{X})}{\partial X_2} & \cdots & \frac{\partial F_2(\mathbf{X})}{\partial X_n} \\ \vdots & \vdots & \ddots & \vdots \\ \frac{\partial F_n(\mathbf{X})}{\partial X_1} & \frac{\partial F_n(\mathbf{X})}{\partial X_2} & \cdots & \frac{\partial F_n(\mathbf{X})}{\partial X_n} \end{bmatrix}$$

Subtracting $\mathbf{F}(\mathbf{X}_Q)$ from both sides of (4), we obtain the linear system

$$\dot{\mathbf{x}} = \mathbf{J}_F(\mathbf{X}_Q)\mathbf{x} \quad (5)$$

where the Jacobian matrix is evaluated at \mathbf{X}_Q .

This *linearization* describes the behavior of the circuit in the vicinity of \mathbf{X}_Q ; we call this the *local* behavior. The linearization is simply the *small-signal equivalent circuit* at the operating point \mathbf{X}_Q . In general, the local behavior of a system depends on the operating point \mathbf{X}_Q . For example, a pn-junction diode exhibits a small incremental resistance under forward bias but a large small-signal resistance under reverse bias. Note that for a *linear* or *affine* system, however, the Jacobian matrix \mathbf{J}_F is *independent* of \mathbf{X}_Q ; it is simply the system matrix \mathbf{A} .

Returning to our example of the parallel RLC circuit, a small perturbation (i_3, v_2) about a point (I_3, V_2) is described by

$$\frac{di_3}{dt} = -\frac{1}{L}v_2 \quad (6)$$

$$\frac{dv_2}{dt} = \frac{1}{C_2}i_3 - \frac{G}{C_2}v_2. \quad (7)$$

Note that the global behavior of the parallel RLC circuit described by (2) and (3) has precisely the same form as the local behavior (6) and (7) at *every* point (I_3, V_2) in the state space. This is a unique property of linear systems.

Stability: Qualitatively, an equilibrium point is said to be *stable* if trajectories starting close to it remain nearby for all future time [17] and *unstable* otherwise.

If \mathbf{X}_Q is an *equilibrium point* of (1), a complete description of its *stability* is contained in the eigenvalues of the linearization of (1) about \mathbf{X}_Q . These are defined as the roots λ of the *characteristic equation*

$$\det(\lambda\mathbf{I} - \mathbf{J}_F(\mathbf{X}_Q)) = 0 \quad (8)$$

where \mathbf{I} is the identity matrix.

If none of the eigenvalues of $\mathbf{J}_F(\mathbf{X}_Q)$ has a positive real part, and those that have zero real parts are simple zeros³ of (8), then the equilibrium point \mathbf{X}_Q is classified as *stable*. If the real parts of all of the eigenvalues are strictly negative, the equilibrium point is *asymptotically stable* and is called a *sink* because all nearby trajectories converge toward it.

If *any* of the eigenvalues has a positive real part, the equilibrium point is *unstable*; if *all* of the eigenvalues have positive real parts, the equilibrium point is called a *source*.

Returning to our example, the stability of the single equilibrium point $(0,0)$ of the parallel RLC circuit is completely

³ A *simple zero* of the characteristic equation has multiplicity one.

determined by the eigenvalues of

$$\mathbf{J}_{\mathbf{F}}(0,0) = \mathbf{J}_{\mathbf{F}} = \begin{bmatrix} 0 & -\frac{1}{L} \\ \frac{1}{C_2} & -\frac{G}{C_2} \end{bmatrix}.$$

The characteristic equation is

$$\det(\lambda\mathbf{I} - \mathbf{J}_{\mathbf{F}}) = \lambda^2 + \frac{G}{C_2}\lambda + \frac{1}{LC_2} = 0.$$

The eigenvalues are thus

$$\lambda = -\frac{G}{2C_2} \pm \sqrt{\left(\frac{G}{2C_2}\right)^2 - \frac{1}{LC_2}}.$$

Node, Focus, and Center: Because of our assumption that L and C_2 are both positive, the term under the square root is smaller than $|G/(2C_2)|$.

If $G^2/(4C_2) > 1/L$, then both eigenvalues are real. If, in addition, G is positive, then the real eigenvalues are both negative, and the origin is a *stable node*; the resonant circuit is said to be *overdamped*. If G is negative, both eigenvalues are positive, and the origin is an *unstable node*.

If $G^2/(4C_2) < 1/L$, then the eigenvalues of $\mathbf{J}_{\mathbf{F}}$ are complex conjugates. If G is positive, they have negative real parts, and the equilibrium point is a *stable focus*; the time waveform is a sinusoid with an exponentially decaying envelope. If G is negative, they have positive real parts, and the equilibrium point is an *unstable focus*; the corresponding time waveform is a sinusoid with an exponentially increasing amplitude.

Consider the parallel RLC circuit once more, with $L = 18$ mH and $C_2 = 100$ nF as before. We find that the origin is a stable focus (trajectories spiral toward it) if $G = 500\mu\text{S}$, and an unstable focus (trajectories spiral away from it) if $G = -500\mu\text{S}$. In the special case that $G \equiv 0$, the eigenvalues are purely imaginary, and $\mathbf{X}_{\mathbf{Q}}$ is called a *center* and is said to have *neutral stability*; the corresponding steady-state⁴ solution is a sinusoidal oscillation (again, see Fig. 4).

Energy Considerations: If our RLC circuit has an asymptotically stable equilibrium point (a *sink*) at the origin, energy is dissipated until none remains in the system; thus, every initial condition converges to the origin and the steady-state solution is $I_3 = V_2 = 0$.

Similarly, if the circuit has an unstable equilibrium point at the origin, energy is pumped into the system, and every trajectory diverges from the origin. This is a nonphysical solution. No real circuit can exhibit an unbounded solution since this would require that the energy stored in the system should increase indefinitely. This energy is provided by the *active* (negative) resistor; every physical resistor is *eventually passive* [16], meaning that for a large enough voltage across its terminals, it dissipates power. This in turn limits the maximum values of $|I_3|$ and $|V_2|$.

In the special case of zero damping, the system is called *conservative*. The energy of the circuit is constant; it merely oscillates back and forth between the energy-storage elements. The voltage and current waveforms are sinusoidal of the form

⁴The *steady-state* solution is the behavior after any initial transient has died out.

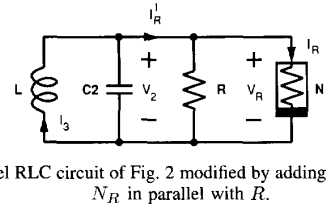


Fig. 5. Parallel RLC circuit of Fig. 2 modified by adding a nonlinear resistor N_R in parallel with R .

$I_3 = A \cos(\omega t + \phi)$ and $V_2 = A \sqrt{L/C_2} \sin(\omega t + \phi)$, where $\omega = 1/\sqrt{LC_2}$ and A and ϕ are determined by the initial conditions.

Sinusoidal Solutions, Structural Stability, and Bifurcations: The way to characterize a sinusoid is to specify its frequency and amplitude. The radial frequency of the oscillation in the undamped parallel RLC resonant circuit is defined by the parameters of the circuit: $\omega = 1/\sqrt{LC_2}$. Because the *amplitude* is specified by the initial conditions, two different sets of initial conditions will usually produce two different sinusoids. Mathematically, we say that the sinusoidal solution of the linear RLC circuit is *not structurally stable*.

Structural stability refers to the sensitivity of a phenomenon to small changes in the parameters of the system. In the parallel RLC circuit, the steady-state solution is a sinusoidal oscillation only if G is *identically equal to zero*. If G is negative, the amplitude of the oscillation grows exponentially; if G is positive, the amplitude decays to zero. In the special case when $G \equiv 0$, the slightest perturbation of G will turn the equilibrium point into a source or a sink. If we think of the system as being parametrized by G , then the vector field is not structurally stable at $G = 0$. We say that the equilibrium point undergoes a *bifurcation* (from stability to instability) as the value of the *bifurcation parameter* G is increased through the *bifurcation point* $G = 0$.

We know from experience that most real-world oscillations are insensitive to small perturbations; they are structurally stable. Therefore, although a linear RLC circuit provides a convenient model for analysis purposes, it represents a poor model of reality. A real oscillator must possess a nonlinearity to control the amplitude of the oscillation.

Thus, if we are to develop insights into oscillatory phenomena, we must appreciate the fundamental role of nonlinearity in the process.

IV. CONTINUOUS CHAOS NEEDS THREE DEGREES OF FREEDOM

We have seen that steady-state sinusoidal oscillation in the linear parallel RLC circuit is not a structurally stable phenomenon. In this section, we add a nonlinearity to the resistive part of the circuit in order to produce sustained periodic oscillation. The most natural extension of linear theory to the world of nonlinear circuits is through piecewise-linear modeling. Therefore, we modify the parallel RLC circuit by placing in parallel with R a piecewise-linear nonlinear resistor N_R , as shown in Fig. 5.

The driving-point (DP) characteristic of N_R (shown in Fig. 6) is defined analytically by

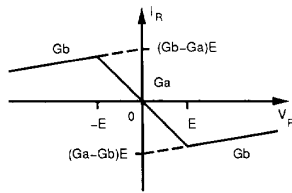


Fig. 6. Driving-point characteristic of the nonlinear resistor N_R shown in Fig. 5.

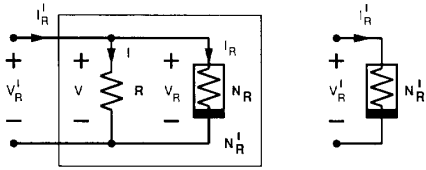


Fig. 7. Parallel combination of R and N_R is equivalent to a single nonlinear resistor N'_R .

$$I'_R = f(V'_R) = \begin{cases} G_b V'_R + (G_b - G_a)E & \text{if } V'_R < -E \\ G_a V'_R & \text{if } -E \leq V'_R \leq E \\ G_b V'_R + (G_a - G_b)E & \text{if } V'_R > E \end{cases}$$

where $E > 0$, $G_b > 0$, and $G_a < 0$.

We can simplify this circuit by combining the two resistive elements R and N_R into a single nonlinear resistor N'_R that has the same DP characteristic [16] (see Fig. 7).

The DP characteristic of N'_R may be determined *analytically* by applying Kirchhoff's laws. Consider Fig. 7; we have that $V'_R = V = V_R$ and $I'_R = I + I_R$. Thus

$$\begin{aligned} I'_R &= G V'_R + f(V'_R) \\ &= f'(V'_R) \\ &= \begin{cases} G'_b V'_R + (G_b - G_a)E & \text{if } V'_R < -E \\ G'_a V'_R & \text{if } -E \leq V'_R \leq E \\ G'_b V'_R + (G_a - G_b)E & \text{if } V'_R > E \end{cases} \end{aligned} \tag{9}$$

where $G'_a = (G + G_a)$ and $G'_b = (G + G_b)$.

The DP characteristic of N'_R may also be determined *graphically* by adding the characteristics of R and N_R *vertically*; for each value of V'_R , add the corresponding values of I and I'_R [16]. We demonstrate this graphical procedure in Fig. 8 for two typical cases: $G'_a < 0$ and $G'_a > 0$.

4.1. Piecewise-Linear Description of the Circuit

Combining R and N_R into a single nonlinear resistor N'_R , we obtain the reduced equivalent circuit shown in Fig. 9. This circuit may be described by a pair of ordinary differential equations. Choosing I_3 and V_2 as *state variables*, as before,

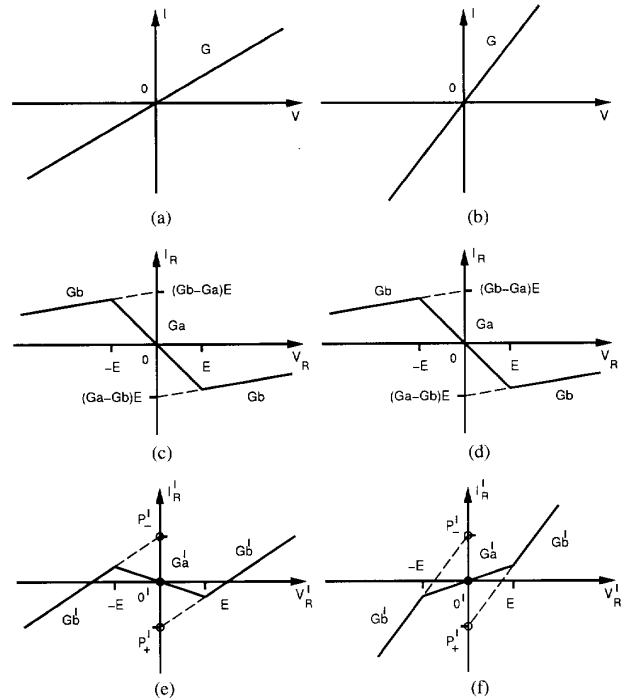


Fig. 8. DP characteristic of N'_R may be determined graphically by adding the characteristics of R and N_R as shown. By Kirchhoff's laws, $V'_R = V = V_R$ and $I'_R = I + I_R$. When $G'_a < 0$, the characteristics of resistor R (a) and N_R (b) sum to give a nonmonotone characteristic (c). When $G'_a > 0$, the characteristics of resistor R (d) and N_R (e) sum to give a monotone v - i characteristic (f).

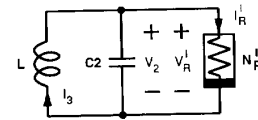


Fig. 9. Simplified equivalent circuit for Fig. 5 obtained by grouping R and N_R into an equivalent resistor N'_R with DP characteristic defined by (9).

we write

$$\begin{aligned} \frac{dI_3}{dt} &= -\frac{1}{L} V_2 \\ \frac{dV_2}{dt} &= \frac{1}{C_2} I_3 - \frac{1}{C_2} I'_R \\ &= \begin{cases} \frac{1}{C_2} I_3 - \frac{G'_b}{C_2} V_2 - \left(\frac{G_b - G_a}{C_2}\right)E & \text{if } V_2 < -E \\ \frac{1}{C_2} I_3 - \frac{G'_a}{C_2} V_2 & \text{if } -E \leq V_2 \leq E \\ \frac{1}{C_2} I_3 - \frac{G'_b}{C_2} V_2 - \left(\frac{G_a - G_b}{C_2}\right)E & \text{if } V_2 > E \end{cases} \end{aligned}$$

Piecewise-linear analysis is a means by which the state space of a nonlinear dynamical system is divided into a set of separate affine regions that may be studied in isolation and then "glued together" along their boundaries. In this case, our circuit may be decomposed into three distinct affine regions: $V_2 < -E$, $|V_2| \leq E$, and $V_2 > E$. We call these the D'_{-1} , D'_0 , and D'_1 regions, respectively.

Using piecewise-linear analysis, we examine each region separately and then glue the pieces together. We look at the middle region first.

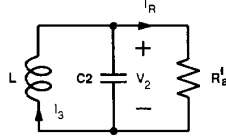


Fig. 10. Equivalent circuit of Fig. 5 in the D'_0 region. $R'_a = 1/G'_a = 1/(G + G_a)$.

4.2. The Middle Region ($|V_2| \leq E$)

When $|V_2| \leq E$, the circuit is described by

$$\begin{aligned} \frac{dI_3}{dt} &= -\frac{1}{L}V_2 \\ \frac{dV_2}{dt} &= \frac{1}{C_2}I_3 - \frac{G'_a}{C_2}V_2 \end{aligned}$$

The D'_0 equivalent circuit is simply the linear parallel RLC circuit shown in Fig. 10.

This linear circuit has a single equilibrium point $0'$ at the origin whose stability is completely specified by the eigenvalues of

$$\mathbf{J}_{\mathbf{F}'_a} = \begin{bmatrix} 0 & -\frac{1}{L} \\ \frac{1}{C_2} & -\frac{G'_a}{C_2} \end{bmatrix}$$

namely

$$\lambda = -\frac{G'_a}{2C_2} \pm \sqrt{\left(\frac{G'_a}{2C_2}\right)^2 - \frac{1}{LC_2}}$$

Our standing assumption that L and C_2 are both positive ensures that the real parts of both eigenvalues are *negative* when G'_a is positive. The system has *positive* damping in this region, and $0'$ is a *stable* equilibrium point; trajectories in D'_0 move *toward* the origin. If $G'_a < 0$, the real parts of both eigenvalues are *positive*; the equilibrium point is then *unstable*, and trajectories move *away* from the origin.

4.3. The Outer Regions ($|V_2| > E$)

In the outer regions, the piecewise-linear circuit of Fig. 5 is described by

$$\begin{aligned} \frac{dI_3}{dt} &= -\frac{1}{L}V_2 \\ \frac{dV_2}{dt} &= \frac{1}{C_2}I_3 - \frac{G'_b}{C_2}V_2 - \frac{1}{C_2}I' \end{aligned} \quad (10)$$

where $I' = (G_b - G_a)E$ when $V_2 < -E$ (the D'_{-1} region) and $I' = (G_a - G_b)E$ when $V_2 > E$ (the D'_1 region).

The D'_{-1} and D'_1 affine equivalent circuits⁵ consist of a linear parallel RLC circuit with resistance $R'_b = 1/G'_b$ and a shunt dc current source I' , as shown in Fig. 11.

The equilibrium points P'_- and P'_+ (dc solutions) of the D'_{-1} and D'_1 equivalent circuits are $(I_{3P'_-}, V_{2P'_-}) = ((G_b - G_a)E, 0)$, and $(I_{3P'_+}, V_{2P'_+}) = ((G_a - G_b)E, 0)$, respectively. We remark that these equilibrium points are simply the points

⁵ The D'_{-1} and D'_1 equivalent circuits are not small-signal (local) equivalent circuits; they model the *large-signal* (global) behavior of the system in the outer regions.

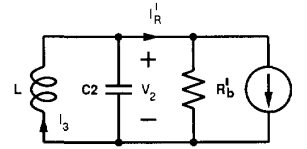


Fig. 11. Equivalent circuit of Fig. 5 for the outer regions. $R'_b = 1/G'_b = 1/(G + G_b)$. $I' = (G_b - G_a)E$ when $V_2 < -E$ and $I' = (G_a - G_b)E$ when $V_2 > E$.

of intersection of the DP characteristic of N'_R with the I'_R axis, as indicated in Fig. 8.

If the equilibrium point of the D'_{-1} equivalent circuit lies *outside* the D'_{-1} region, then it is called a *virtual* equilibrium point (denoted by an open circle in Fig. 8). Although this is a valid solution of the affine D'_{-1} equivalent circuit described by (10), it is not an equilibrium point of the *piecewise-linear* circuit itself.

We can determine the stability of the equilibrium points and the dynamics of the outer regions by examining the Jacobian matrix

$$\mathbf{J}_{\mathbf{F}'_b} = \begin{bmatrix} 0 & -\frac{1}{L} \\ \frac{1}{C_2} & -\frac{G'_b}{C_2} \end{bmatrix}$$

whose eigenvalues are

$$\lambda = -\frac{G'_b}{2C_2} \pm \sqrt{\left(\frac{G'_b}{2C_2}\right)^2 - \frac{1}{LC_2}}$$

With $G'_b > 0$, the circuit has positive damping in the outer regions and a trajectory will converge *toward* the corresponding virtual equilibrium until it crosses the boundary and enters the D'_0 region.

4.4. Global Behavior

The vector field for the piecewise-linear circuit in Fig. 5 is formed by gluing together the vector fields of the three regions D'_{-1} , D'_0 , and D'_1 . This is illustrated in Fig. 12.

We consider two cases in detail: $G'_a > 0$ and $G'_a < 0$. In each case, the circuit has a unique equilibrium point $0'$ at the origin.

If $G'_a > 0$, the circuit is dissipative everywhere, and all trajectories collapse toward the inner region. The unique steady-state solution of the circuit is the stable dc equilibrium condition $I_3 = V_2 = 0$.

If $G'_a < 0$, the equilibrium point at the origin is *unstable*, and the vector field in the D'_0 region pushes trajectories *away* from it. In the outer regions, trajectories are pulled by the dissipative vector field *toward* the corresponding virtual equilibria P'_- and P'_+ . The resulting balance of forces produces a periodic steady-state trajectory called a *limit cycle*, which is approached asymptotically by all initial conditions of this circuit.

This limit cycle is termed *attracting* (stable) because nearby trajectories move *toward* it and is *structurally stable* in the sense that a small change in the parameters of the circuit has little effect on it.

The *basin of attraction* of a stable limit cycle is the set of all initial conditions from which trajectories converge to the

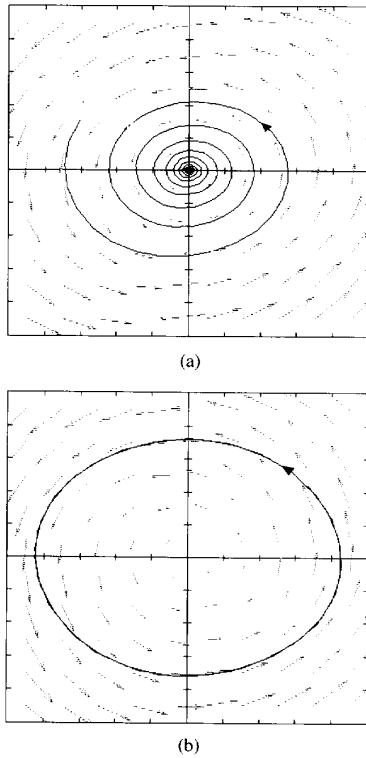


Fig. 12. Vector fields for the nonlinear RLC circuit in Fig. 14. $L = 18\text{mH}$, $R_0 = 12.5\Omega$, $C_2 = 100\text{nF}$, $G_a = -757.576\mu\text{S}$, $G_b = 45.455\mu\text{S}$, $E = 0.47\text{V}$. (a) $G = 1\text{mS}$: all trajectories converge to the origin. (b) $G = 500\mu\text{S}$: the unique steady-state solution is a limit cycle. Horizontal axis: I_3 , $400\mu\text{A}/\text{div}$; vertical axis: V_2 , $200\text{mV}/\text{div}$.

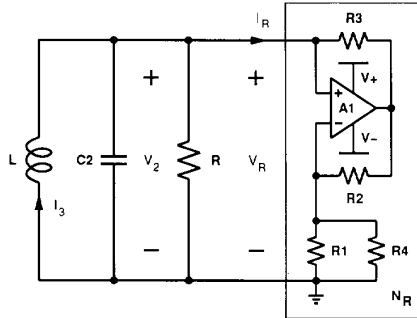


Fig. 13. Piecewise-linear oscillator circuit. L is a wirewound inductor (TOKO type 10RB or equivalent) with nominal inductance 18mH and a measured series resistance of 12.5Ω . C_2 is a 100-nF capacitor. R is a $2\text{k}\Omega$ multium potentiometer. A_1 is a BiFET operational amplifier (Analog Devices type AD712, Texas Instruments type TL082, or equivalent). R_1 is a $3.3\text{k}\Omega$ resistor, R_2 and R_3 are $22\text{k}\Omega$ resistors, and R_4 is a $2.2\text{k}\Omega$ resistor.

limit cycle. The basin of attraction of the limit cycle when $G'_a < 0$ is the *entire* state space.

4.5. Laboratory Experiment: Piecewise-Linear Oscillator with One Equilibrium Point

In this experiment, we demonstrate the concepts outlined above: an *equilibrium point*, *stability*, a *bifurcation*, and a *limit cycle*.

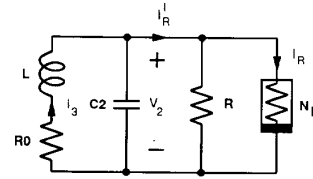


Fig. 14. Equivalent circuit for Fig. 13. The series resistance of the inductor is modeled by R_0 .

Circuit Description: Consider the op-amp based oscillator circuit shown in Fig. 13. The subcircuit N_R consisting of A_1 and R_1 – R_4 ⁶ may be modeled by a nonlinear resistor N_R with driving-point characteristic as shown in Fig. 6 [14]. When $R_2 = R_3$, $G_a = -1/R_1 - 1/R_4$, $G_b = 1/R_3$, and $E = R_1 R_4 E_{sat} / (R_1 R_2 + R_1 R_4 + R_2 R_4)$, where E_{sat} is the saturation level of the op amp. With $R_2 = R_3 = 22\text{k}\Omega$, $R_1 = 3.3\text{k}\Omega$, $R_4 = 2.2\text{k}\Omega$, and $E_{sat} = 8.3\text{V}$, $G_a = -50/66\text{mS} = -757.576\mu\text{S}$, $G_b = 1/22\text{mS} = 45.455\mu\text{S}$, and $E \approx 0.47\text{V}$.

R in parallel with N_R is equivalent to a single nonlinear resistor N'_R whose DP characteristic is shown in Fig. 8. By varying the conductance of the potentiometer R , we can adjust the slopes G'_a and G'_b of this characteristic.

The simplified equivalent circuit is shown in Fig. 14. Here, we model the real inductor as a series connection of an ideal linear inductor L and a linear resistance R_0 .⁷

Steady-State Solutions:

Stable equilibrium point: Consider the case when R is 0Ω ; this is equivalent to short circuiting the LC resonant circuit. The unique solution ($V_2 = I_3 = 0$) corresponds to a dc equilibrium point at the origin.

Bifurcation and limit cycle: Increase R until the equilibrium point at the origin undergoes a bifurcation and becomes unstable; at this point, the circuit begins to oscillate. Increasing R further causes the oscillation to increase in amplitude.

Measured typical steady-state behaviors are shown in Fig. 15.

4.6. Uniqueness of Solution

We have seen that depending on the parameters, this circuit can have a stable equilibrium point or limit cycle as a solution. Can it exhibit more complicated steady-state behavior?

Because the vector field is uniquely defined and trajectories of the system are tangent to the vector field everywhere, a trajectory cannot cross itself [18]. The implication of this is that a second-order autonomous circuit whose trajectories lie in the plane can exhibit just two types of steady-state behavior: an equilibrium point or a limit cycle.

A different choice of nonlinearity in this example might yield more equilibrium points or limit cycles, but an autonomous circuit containing just two energy storage elements

⁶We show two resistors R_1 and R_4 in parallel rather than a single resistor of 1320Ω simply because we wish to use the same set of components in all of the experiments in this two-part paper.

⁷If R_0 is sufficiently small, it has negligible qualitative effect on the global behavior of the circuit.

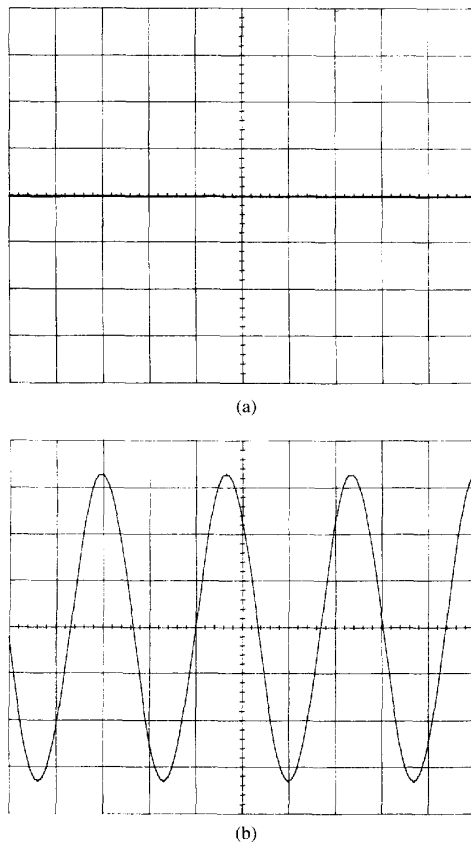


Fig. 15. Measured steady-state behaviors for the experimental circuit shown in Fig. 13. $L = 18$ mH, $R_0 = 12.5\Omega$, $C_2 = 100$ nF, $G_a = -757.576\mu\text{S}$, $G_b = 45.455\mu\text{S}$, $E = 0.47$ V. (a) $R = 0\Omega$: The unique steady-state solution is a dc equilibrium point at the origin. (b) $R = 2000\Omega$ ($G = 500\mu\text{S}$): The unique steady-state solution is a limit cycle. Horizontal axis: time, $100\mu\text{s}/\text{div}$; vertical axis: $V_2(t)$, $200\text{ mV}/\text{div}$.

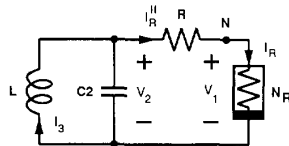


Fig. 16. Nonlinear RLC circuit with R in series with N_R .

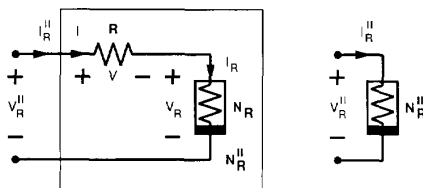


Fig. 17. Series combination of R and N_R in Fig. 16 is equivalent to a single nonlinear resistor N_R'' whose DP characteristic is shown in Fig. 18.

cannot produce a steady-state behavior that is more complicated than this.⁸ In particular, a continuous system described

⁸The only possible solutions of an autonomous 2-D dynamical system are equilibrium points, closed orbits, and unions of equilibrium points and the trajectories connecting them; of these, only equilibrium points and limit cycles are structurally stable (see [17], [4]).

by an autonomous second-order differential equation cannot exhibit chaos; for that, we need at least three degrees of freedom.

V. CONTINUOUS-TIME CHAOS NEEDS A HORSESHOE

Thus far, we have seen that a *linear* parallel RLC resonant circuit cannot produce structurally stable oscillations. The addition of a single nonlinear element causes the circuit to exhibit robust periodic oscillation or a dc solution but nothing more complicated than this. By confining the circuit's dynamics to a 2-D state space, we have limited its possible steady-state behaviors.

In order to produce more complex dynamics, we use the *same* building blocks as before but follow a slightly different evolutionary path from the RLC circuit. This time, instead of placing the nonlinear resistor N_R in parallel with R , we connect it in *series*, as shown in Fig. 16. This minor rearrangement of our four components leads to a fundamental change in the dynamics of the circuit, as we shall see.

Once again, we try to simplify the analysis by replacing the series combination of R and N_R by a single nonlinear resistor N_R'' that has the same DP characteristic. Unlike in the previous case, where the DP characteristic of the equivalent resistor N_R' could be written in terms of the port variables, the current I_R'' into N_R'' cannot always be written explicitly as a function of the voltage (or current) across its terminals. Nevertheless, we can still express the driving-point characteristic of the compound resistor N_R'' by means of a parametric representation in V_R :

$$I_R'' = \begin{cases} G_b'' V_R'' + \frac{G(G_b - G_a)}{G + G_b} E & \text{if } V_R < -E \\ G_a'' V_R'' & \text{if } -E \leq V_R \leq E \\ G_b'' V_R'' + \frac{G(G_a - G_b)}{G + G_b} E & \text{if } V_R > E \end{cases} \quad (11)$$

where $V_R (= V_R'' - V)$ is the voltage across the terminals of N_R (see Fig. 17), $G_a'' = GG_a/(G + G_a)$, and $G_b'' = GG_b/(G + G_b)$. Note that G_a'' is simply the equivalent conductance of the series connection of R and $1/G_a$ and that G_b'' is the equivalent conductance of R and $1/G_b$ in series.

The DP characteristic of N_R'' may be determined graphically by adding the v - i characteristics of R and N_R *horizontally* as dictated by Kirchhoff's laws [16]: For each value of $I_R'' (= I = I_R)$, add the corresponding values of V and V_R as shown in Fig. 18 for two cases: $G_a'' < 0$ and $G_a'' > 0$.

What happens in practice if one tries to measure the driving-point characteristic of the series combination of R and N_R by increasing either the voltage across or current into the terminals is that one observes a "hysteresis" effect [19]. This apparent "hysteresis" is due to the fact that the model of a real nonmonotone voltage-controlled nonlinear resistor such as N_R must always include a parasitic *transit capacitance* across the terminals of the resistor [20]. In the following discussion, we will proceed as far as we can by ignoring this fact until the transit capacitance is forced on us by our inability to explain the circuit's dynamics when it is omitted.

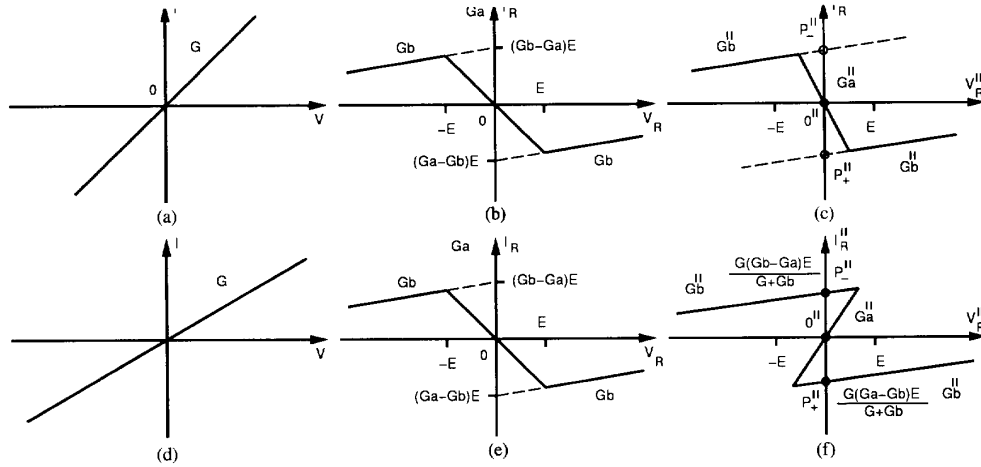


Fig. 18. DP characteristic of N''_R can be determined graphically by adding the characteristics of R and N_R as shown. By Kirchhoff's laws, $I'_R = I = I_R$ and $V''_R = V + V_R$. When $G''_a < 0$, the characteristics of resistor R (a) and N_R (b) sum to give a voltage-controlled characteristic (c). When $G''_a > 0$, the characteristic that results from the addition of (d) and (e) is neither voltage-controlled nor current-controlled (f).

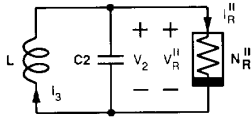


Fig. 19. Simplified equivalent circuit for Fig. 16 obtained by grouping R and N_R into an equivalent resistor N''_R with DP characteristic given defined by (11).

5.1. Piecewise-Linear Description of the Circuit

Choosing I_3 and V_2 as state variables, the nonlinear RLC circuit in Fig. 16 may be described by two state equations

$$\frac{dI_3}{dt} = -\frac{1}{L}V_2 \quad (12)$$

$$\begin{aligned} \frac{dV_2}{dt} &= \frac{1}{C_2}I_3 - \frac{1}{C_2}I''_R \\ &= \frac{1}{C_2}I_3 - \frac{G}{C_2}(V_2 - V_1) \end{aligned} \quad (13)$$

and an algebraic equation relating V_2 and V_1 :

$$0 = G(V_2 - V_1) - f(V_1) \quad (14)$$

This algebraic equation is simply an expression of Kirchhoff's current law (KCL) at node N in Fig. 16; it represents a *constraint* that V_1 (and V_2) must satisfy while the dynamics of the circuit evolve in the 2-D (I_3, V_2) state space.

We have seen that the series combination of R and N_R is equivalent to a single nonlinear resistor N''_R with DP characteristic as shown in Fig. 18. Thus, we can substitute N''_R for the series combination of R and N_R in Fig. 16; this yields the simplified piecewise-linear equivalent circuit shown in Fig. 19. We now decompose this circuit into its three affine regions and consider the behavior in each region separately. We first look at the outer regions, which we denote D''_{-1} and D''_1 .

5.2. The Outer Regions $|V_1| > E$

When $V_1 < -E$ (the D''_{-1} region), the algebraic constraint (14) becomes $G(V_2 - V_1) = G_b V_1 + (G_b - G_a)E$. Solving (14) for V_1 in terms of V_2 and substituting into (13), we find that trajectories of the circuit evolve according to

$$\frac{dI_3}{dt} = -\frac{1}{L}V_2 \quad (15)$$

$$\frac{dV_2}{dt} = \frac{1}{C_2}I_3 - \frac{G''_b}{C_2}V_2 - \frac{1}{C_2}I'' \quad (16)$$

where $I'' = G(G_b - G_a)E/(G + G_b)$.

The equivalent circuit for the D''_{-1} region is the affine parallel RLC circuit shown in Fig. 20. The D''_1 equivalent circuit has the same form but with $I'' = G(G_a - G_b)E/(G + G_b)$.

The D''_{-1} region has an equilibrium point at $(I_{3P''}, V_{2P''}) = (G(G_b - G_a)E/(G + G_b), 0)$ and the D''_1 region has an equilibrium point at $(I_{3P''}, V_{2P''}) = (G(G_a - G_b)E/(G + G_b), 0)$. We remark that these equilibrium points are simply the points of intersection of the DP characteristic of N''_R with the I''_R axis, as shown in Fig. 18(c) and (f). As before, if they lie within their respective domains of applicability, they are true equilibrium points (denoted by solid discs P''_- and P''_+ in Fig. 18(f)); if not, they are called *virtual equilibria* (which we denote by circles in Fig. 18(c)).

The dynamics of the outer regions are determined by the Jacobian matrix:

$$\mathbf{J}_{\mathbf{F}''} = \begin{bmatrix} 0 & -\frac{1}{L} \\ \frac{1}{C_2} & -\frac{G''_b}{C_2} \end{bmatrix}.$$

The eigenvalues of the equilibrium points P''_- and P''_+ are

$$\lambda = -\frac{G''_b}{2C_2} \pm \sqrt{\left(\frac{G''_b}{2C_2}\right)^2 - \frac{1}{LC_2}}.$$

With our standing assumption that C and L_2 are both positive, we make the following observations. When $G''_b > 0$, the circuit has positive damping in the outer regions, and a

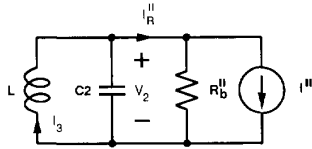


Fig. 20. Equivalent circuit of Fig. 16 for the outer regions. $R_b'' = 1/G_b'' = (G + G_b)/(GG_b)$. This circuit has a unique equilibrium point $(I_3, V_2) = (I'', 0)$. When $R_b'' > 0$, the equilibrium point is *stable*.

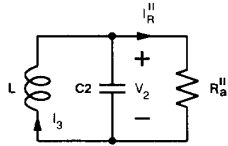


Fig. 21. Equivalent circuit of Fig. 16 for the D_0'' region. $R_a'' = 1/G_a'' = (G + G_a)/(GG_a)$. When $R_a'' < 0$ (Fig. 18(c)), the equilibrium point at the origin is *unstable*; when $R_a'' > 0$ (Fig. 18(f)), the circuit is *stable*.

trajectory will converge *toward* the corresponding equilibrium point. When $G_b'' < 0$, the circuit has negative damping in the outer regions, and a trajectory will diverge *from* the corresponding equilibrium point. In the following discussion, we consider only the case when $G_b'' > 0$; this corresponds to $R_b'' > 0$ in the equivalent circuits for the outer regions (Fig. 20).

5.3. The Middle Region $|V_1| \leq E$

When $|V_1| \leq E$, $f(V_1) = G_a V_1$ and (14) reduces to $G(V_2 - V_1) = G_a V_1$. Substituting for V_1 in (13), the circuit may be modeled as a 2-D dynamical system:

$$\begin{aligned} \frac{dI_3}{dt} &= -\frac{1}{L}V_2 \\ \frac{dV_2}{dt} &= \frac{1}{C_2}I_3 - \frac{G_a''}{C_2}V_2 \end{aligned}$$

The D_0'' equivalent circuit is simply the linear parallel RLC circuit shown in Fig. 21. This circuit has a single equilibrium point at the origin whose stability may be determined by analyzing the Jacobian matrix

$$\mathbf{J}_{F_a}'' = \begin{bmatrix} 0 & -\frac{1}{L} \\ \frac{1}{C_2} & -\frac{G_a''}{C_2} \end{bmatrix}$$

whose eigenvalues are

$$\lambda = -\frac{G_a''}{2C_2} \pm \sqrt{\left(\frac{G_a''}{2C_2}\right)^2 - \frac{1}{LC_2}}$$

Now, if G_a'' is positive (corresponding to Fig. 18(f)), the real parts of both eigenvalues are *negative*, the D_0 equivalent circuit has *positive* damping, and the origin is *stable*. Trajectories in D_0'' move *toward* the origin.

If G_a'' is negative (corresponding to Fig. 18(c)), the real parts of both eigenvalues are *positive*, and the origin is therefore *unstable*. When $|V_2| < E$, the circuit system has *negative* damping, and trajectories move *away* from the origin.

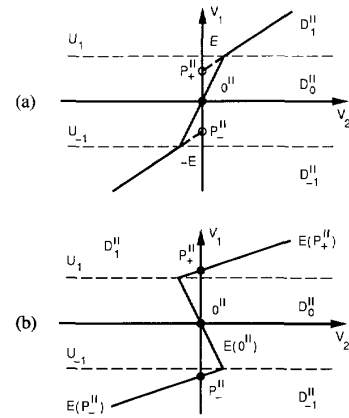


Fig. 22. Relationship between V_1 and V_2 : $G(V_2 - V_1) - f(V_1) = 0$: (a) When $G_a'' < 0$, V_1 is uniquely determined by V_2 ; (b) when $G_a'' > 0$, V_1 cannot be written as a function of V_2 . U_1 is the plane defined by $V_1 \equiv E$; similarly, U_{-1} is the separating plane $V_1 \equiv -E$.

5.4. Global Behavior

In order to gain some intuition on the dynamics in each region, we refer to Figs. 18 and 19 once more. An equilibrium point (dc solution) of Fig. 19 may be found by short circuiting L and open circuiting C_2 ; this is simply a point of intersection of the DP characteristic of N_R'' with the I_R'' axis (where $V_2 = V_R'' = 0$). The *stability* of an equilibrium point is determined by the *slope* of the DP characteristic of N_R'' at that point: If the slope is positive, the equilibrium point is *stable*; if the slope is negative, the equilibrium point is *unstable*.

Referring to Fig. 18(c), we see that points P_-'' and P_+'' are stable virtual equilibria, and the origin is an unstable equilibrium point of Fig. 19 when $G_a'' < 0$. Similarly, we recognize from Fig. 18(f) that P_-'' , $0''$, and P_+'' are all stable equilibria of Fig. 19 when $G_a'' > 0$.

In determining the dynamical behavior of the circuit in each region, we solved (14) for V_1 in terms of V_2 and substituted into (13) to obtain a 2-D equivalent circuit. Consider now the relationship between V_1 and V_2 as expressed by the algebraic constraint (14) and shown graphically in Fig. 22. When $G_a'' < 0$, V_1 is uniquely determined by V_2 but not when $G_a'' > 0$. We consider these two cases in detail.

5.5. $G_a'' < 0$

Equilibrium Points: When $G_a'' < 0$, the dissipative outer regions have stable *virtual* equilibria P_-'' and P_+'' in the D_0'' region (see Fig. 18); the D_0'' region itself has an unstable equilibrium point at the origin. Thus, the circuit has a unique unstable equilibrium point $0''$.

When $G_a'' < 0$, $V_2 = V_1 + f(V_1)/G = g(V_1)$ is a monotone increasing function of V_1 . This enables us to write V_1 explicitly as a function of V_2 and to express the *global* dynamics of the circuit in the form

$$\begin{aligned} \frac{dI_3}{dt} &= -\frac{1}{L}V_2 \\ \frac{dV_2}{dt} &= \frac{1}{C_2}I_3 - \frac{G}{C_2}(V_2 - g^{-1}(V_2)). \end{aligned} \quad (17)$$

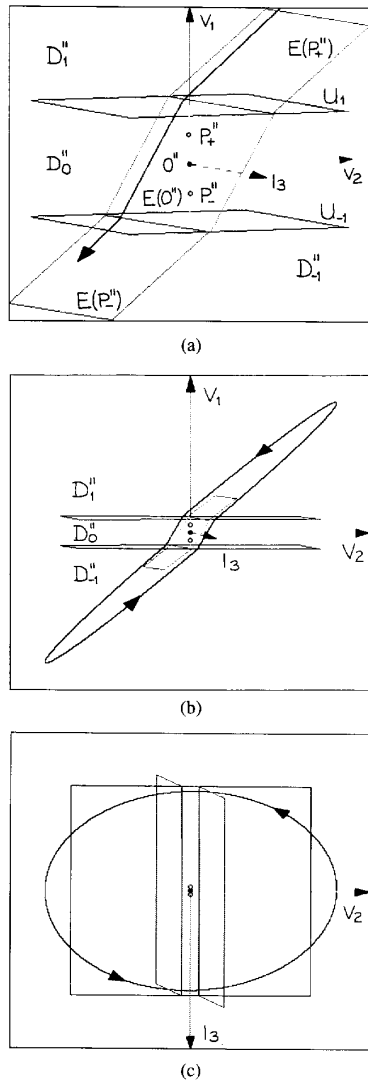


Fig. 23. When $G_a'' > 0$, the planes in the 3-D (I_3, V_2, V_1) coordinate system defined by the constraint (14) meet at *obtuse* angles (a). The circuit of Fig. 16 possesses a single unstable equilibrium point: $0''$ at the origin. Trajectories in the outer regions collapse towards the stable virtual equilibria at P_4'' and P_-'' in the middle region. A trajectory crossing the boundary $V_1 = E$ from the D_1'' region moves slowly through D_0'' and enters D_{-1}'' , where it is turned back and crosses back to D_1'' ; a limit cycle results (b). (c) The projection of this limit cycle onto the I_3 - V_2 plane is a smooth closed curve (the V_2 half axis scale represents 5 V; the I_3 half axis scale is 15 mA).

Geometrical Structure of the Dynamics: In the 3-D (I_3, V_2, V_1) coordinate system, the constraint (14) defines three planes that meet at *obtuse* angles as shown in Fig. 23(a). Note that a cross section through these planes with a constant I_3 is simply the KCL constraint (14), which is shown graphically in Fig. 22(a). In each region, a trajectory is constrained to lie on the corresponding plane that relates V_2 and V_1 .

The global behavior of the circuit can be determined by gluing these planes together. Since we have an explicit ex-

pression for the dynamics in each region, we concern ourselves here with what happens at the boundaries where these planes meet.

A trajectory starting in the D_1'' region moves toward the virtual equilibrium point P_4'' until it crosses into the D_0'' region. Once in the D_0'' region, the trajectory is repelled by the unstable equilibrium point at $0''$ until it crosses into the D_{-1}'' region. By symmetry, this trajectory in the D_{-1}'' region is attracted back toward its virtual equilibrium point P_-'' until it crosses back into the D_0'' region. It is not surprising, therefore, that the resulting steady-state behavior is a stable limit cycle, as shown in Fig. 23(b). Indeed, this *limit cycle* is the unique steady-state solution of this circuit.

The Kink: One can think of the dynamics of this oscillator as similar to that of the previous example with $G_a' < 0$. In that case, the steady-state solution was a limit cycle on a plane. Here, we have introduced a kink (in the V_1 direction) into the (I_3, V_2) plane on which the dynamics are evolving. The 2-D global dynamics (17) is simply the projection of trajectories in the (I_3, V_2, V_1) coordinate system onto the (I_3, V_2) plane, as shown in Fig. 23(c).

5.6. $G_a'' > 0$

Because of the fold in the DP characteristic of N_R'' when $G_a'' > 0$, the vector field described by (12) and (13) can assume any of three different values in the region of overlap, depending on the value of V_1 . Since V_2 is a nonmonotone function of V_1 in this case, V_1 cannot be expressed globally as a function of V_2 . In marked contrast with the previous case, this means that we cannot write global state equations for the circuit when $G_a'' > 0$. Indeed, the circuit no longer behaves in a 2-D manner so that our simplistic 2-D analysis fails. Nevertheless, the problem can be resolved by adding a transit capacitor in parallel with N_R in Fig. 16, as we shall see.

Equilibrium Points: When $G_a'' > 0$, the circuit of Fig. 16 has three equilibrium points that we label P_-'' , $0''$, and P_+'' . With $G_b'' > 0$ and $G_a'' > 0$, our 2-D piecewise-linear analysis suggests that all three equilibrium points are *stable*. One might expect, therefore, that all trajectories would settle to one or other of these stable equilibria. In particular, it should be possible for a trajectory to remain indefinitely at $0''$.

Geometrical Structure of the Dynamics: In the 3-D (I_3, V_2, V_1) coordinate system, the constraint (14) defines three planes that now meet at *acute* angles, as illustrated in Fig. 24(a). Note once again that a cross section through these planes with a constant I_3 is simply the KCL constraint (14), which is shown graphically in Fig. 22(b).

As before, we have explicit expressions for the dynamics in each region. A qualitative picture of the global behavior of the circuit may be gleaned by separately considering the evolution of (12)–(14) in each region and the transitions between regions.

Let us consider a trajectory starting in the D_1'' region with V_2 large enough that the 2-D vector field defined by (12) and (13) is unique. Because the system is dissipative in the outer region, a trajectory evolving on the constraint plane $E(P_+'')$ in the D_1'' region moves toward the equilibrium point at P_+'' , where $E(P_+'')$ is defined by $GV_2 = (G + G_b)V_1 + (G_b - G_a)E$.

Once the trajectory enters the region of overlap in the DP characteristic, the vector field becomes triple valued, and the dynamics are not well defined.

Nevertheless, let us assume that the trajectory remains on $E(P_+''')$ (where its evolution is governed by (15) and (16)) and see what happens. Although it is converging *toward* P_+''' along $E(P_+''')$, this trajectory may reach a point $\mathbf{X}_+ = (I_3', V_2', V_1^+)$ on the separating plane U_1 (defined by $V_1 \equiv E$) between the D_1'' and D_0'' regions *before* it reaches P_+''' .

Now, every trajectory reaching U_1 along $E(P_+''')$ from the D_1'' region has the property that $dV_2/dt \leq 0$ at U_1 .⁹ A trajectory reaching the same boundary point \mathbf{X}_+ from the D_0'' region along $E(0''')$ also has $dV_2/dt \leq 0$ at U_1 . In particular, if dV_2/dt is *negative* at the boundary point, then our assumed trajectory reaching this point from the D_1'' region cannot continue along the constraint plane $E(P_+''')$; \mathbf{X}_+ is called an “impasse point” [21], [22].

The impasse may be resolved by applying the “jump rule” [16]; we postulate that the trajectory reaching U_1 from the D_0'' region at a point (I_3', V_2', V_1^+) on $E(P_+''')$ “jumps” through the D_0'' region to another point $\mathbf{X}_- = (I_3', V_2', V_1^-)$ on the constraint plane $E(P_-''')$ in the D_{-1}'' region that has the same 2-D state (I_3', V_2') . This is illustrated in Fig. 24(a).

If the trajectory crosses repeatedly between the D_{-1}'' and D_1'' regions by jumping through D_0'' , then the steady-state solution of this circuit might be a limit cycle (see Fig. 24(b)).

This solution is not unique, however, since we know from our 2-D analysis that a trajectory starting on the plane $E(P_+''')$ will be attracted toward the equilibrium point P_+''' . In particular, trajectories starting *at* the P_+''' will remain there indefinitely, and trajectories starting close to P_+''' converge asymptotically to the equilibrium point without ever reaching the boundary plane U_1 . Indeed, both P_+''' and P_-''' are *stable* equilibrium points of this circuit.

Consider now a trajectory originating on the plane $E(0''')$ in the D_0'' region (where $E(0''')$ is defined by $GV_2 = (G + G_a)V_1$). Because the DP characteristic of N_R'' has a *positive* slope at the origin when $G_a'' > 0$, the second-order linear equivalent circuit for the middle region is *stable*, and we might expect the origin to be a stable equilibrium point of the circuit shown in Fig. 16. We will see that the origin of this circuit is in fact *unstable* when an arbitrarily small positive parasitic capacitance is added in parallel with N_R .

The Fold: When $G_a'' < 0$, we saw that the resulting geometrical structure was akin to putting a kink in the plane of the vector field; here, $G_a'' > 0$, and we have instead *folded* the planes on which the dynamics of the system are evolving.

The projection of the vector field in each region onto the (I_3, V_2) plane now produces a nonunique (triple valued) vector field in the region of overlap. By definition, the vector field of an autonomous dynamical system must be *unique* at every point in its state space. It is for precisely this reason that the global state equations are undefined. Nevertheless, the projection of the limit cycle (Fig. 24(b)) onto the (I_3, V_2) plane (Fig. 24(c)) is *smooth*; only V_1 experiences jumps.

⁹Consider Fig. 22(b). A trajectory lying along the constraint plane $E(P_+''')$ in the D_1'' region an infinitesimal distance away from the separating plane $V_1 \equiv E$ moves *away* from U_1 if $dV_2/dt > 0$.

Because it is not possible to write global state equations for Fig. 16 when $G_a'' > 0$, we simulated the behavior of the circuit using the augmented circuit shown in Fig. 28 with the following parameter values: $L = 18$ mH; $C_2 = 100$ nF; $G_a = -757.576 \mu\text{S}$; $G_b = 45.455 \mu\text{S}$; $E = 470$ mV. Fig. 24 shows the simulated behavior of the circuit when $G = 1/R = 1.56$ mS ($G_a'' = -1.47$ mS < 0), and Fig. 23 shows the case $G = 500 \mu\text{S}$ ($G_a'' = 1.47$ mS > 0).

In addition to the components of Fig. 16, this circuit contains two parasitic elements: $R_0 = 12.5 \Omega$ that accounts for the series resistance of the real inductor and a parasitic transit capacitor $C_1 = 100$ pF that completes the model of the nonmonotone voltage-controlled resistor N_R and allows us to write well-defined global state equations for the circuit. We will see in the following section that the circuit in Fig. 28 reduces to that in Fig. 16 as $R_0 \rightarrow 0$ and as $C_1 \rightarrow 0$.

VI. THE FINAL EVOLUTIONARY STEP—THE THIRD DIMENSION

In studying the geometry of the (I_3, V_2, V_1) coordinate space of this circuit when $G_a'' > 0$, we noticed that the planes along which the second-order dynamics are evolving meet at acute angles, leading to a fold. In the region of the fold, the dynamics depend explicitly on the “hidden” variable V_1 . By adding an infinitesimal (positive) parasitic transit capacitance C_1 in parallel with N_R , as shown in Fig. 25, we can keep track of V_1 ; the circuit then becomes well defined, and we can write global state equations. Having done this, the circuit is no longer described by a second-order system and an algebraic equation but is now completely described by a system of three ordinary differential equations called Chua’s circuit equations.

$$\frac{dI_3}{dt} = -\frac{1}{L}V_2 \quad (18)$$

$$\frac{dV_2}{dt} = \frac{1}{C_2}I_3 - \frac{G}{C_2}(V_2 - V_1) \quad (19)$$

$$\frac{dV_1}{dt} = \frac{G}{C_1}(V_2 - V_1) - \frac{1}{C_1}f(V_1) \quad (20)$$

6.1. Qualitative Analysis of the Parasitic Dynamics

Because the time constant associated with the infinitesimal (positive) parasitic capacitance C_1 in the third equation is so much smaller than those associated with the first two, this modified circuit is said to possess what are called *slow-fast* dynamics. The fast parasitic dynamics cause trajectories of the circuit in the outer regions to lie on the constraint planes defined by (14) where the dynamics evolve like a 2-D system. Consequently, an analysis of these 2-D dynamics is normally sufficient to understand the operation of the circuit *except at the folds*. At the fold, however, a trajectory reaching an impasse point from one of the outer planes comes under the influence of the “fast” dynamics and “jumps” through the D_0'' region.

To appreciate the jump mechanism, consider (20) with an infinitesimal capacitance C_1 . The right-hand side ($G(V_2 -$

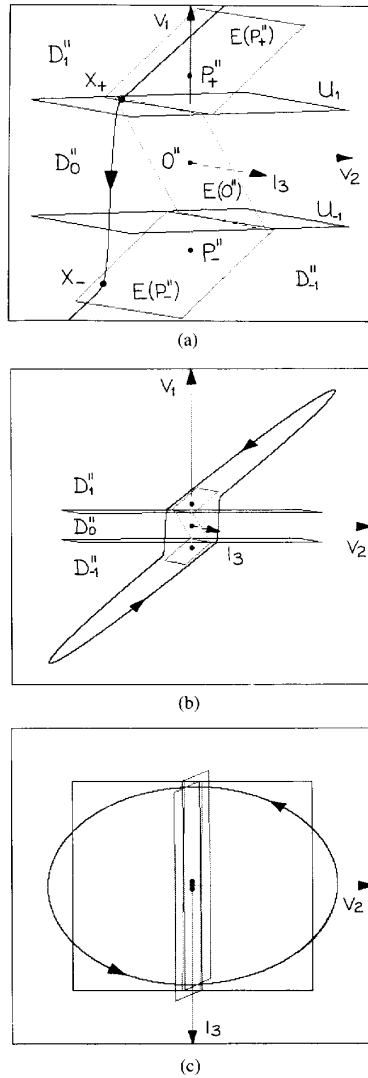


Fig. 24. When $G''_a > 0$, the planes in the 3-D (I_3, V_2, V_1) coordinate system defined by the constraint (14) meet at acute angles (a). The circuit of Fig. 16 possesses three equilibrium points: P_+'' , $0''$ and P_-'' . Trajectories in the outer regions either converge toward the stable equilibria at P_+'' and P_-'' or “jump” repeatedly through the D_0'' region to produce a limit cycle (b). (c) When projected onto the I_3 - V_2 plane, this limit cycle appears as a smooth closed curve (the V_2 half-axis scale represents 5 V; the I_3 half-axis scale is 15 mA).

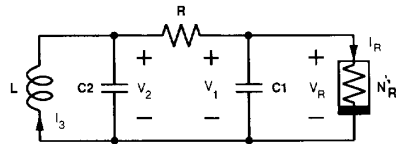


Fig. 25. By adding the necessary parasitic transit capacitance C_1 in parallel with N_R , the circuit of Fig. 16 becomes Chua's circuit.

$V_1) - f(V_1))$ defines a relationship between V_2 and V_1 , as shown in Fig. 22.

If V_2 lies to the left of this curve, $G(V_2 - V_1) - f(V_1) < 0$, $dV_1/dt < 0$, and V_1 decreases with a time constant inversely

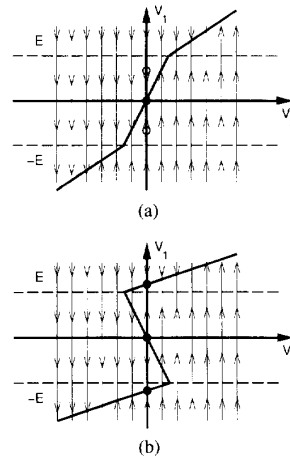


Fig. 26. Parasitic dynamics associated with the oscillator: (a) $G''_a < 0$; (b) $G''_a > 0$. We have added arrows to Fig. 22 to indicate the direction of the V_1 component of the 3-D vector field defined by (18)–(20). When $G(V_2 - V_1) - f(V_1) < 0$, V_1 is decreasing; when $G(V_2 - V_1) - f(V_1) > 0$, V_1 is increasing.

proportional to C_1 until it satisfies the constraint. Similarly, if V_2 lies to the right of the curve, $G(V_2 - V_1) - f(V_1) > 0$, $dV_1/dt > 0$, and V_1 increases with time. If we draw arrows on Fig. 22 to indicate the direction of the component of the 3-D vector field associated with the parasitic dynamics (20), as shown in Fig. 26, we see clearly why a trajectory entering the middle region from the upper region quickly “jumps” across to the other side.

We also realize why the origin is not a stable equilibrium point of the circuit. Although the eigenvalues of J_{F_a}'' suggest that the origin is stable (along the plane defined by $GV_2 = (G + G_a)V_1$) when $G''_a > 0$, the parasitic dynamics in the D_0'' region cause the origin to be unstable “in the V_1 direction.” A trajectory lying on the plane defined by $G(V_2 - V_1) - G_a V_1 = 0$ will converge toward the origin along that plane. However, trajectories above and below the plane will be pushed away toward the outer regions.

6.2. Laboratory Experiment: Piecewise-Linear Oscillator with Multiple Equilibria

In this experiment, we demonstrate the concepts of multiple equilibria, multiple solutions, bistability, and limit cycles.

Circuit Description: Consider the circuit shown in Fig. 27. The potentiometer R is now in series with the nonlinear resistor N_R , giving an effective driving point characteristic as shown in Fig. 18. The subcircuit N_R consisting of A_1 and R_1 – R_4 may be modeled as before by a nonlinear resistor with driving-point characteristic as shown in Fig. 6.

The equivalent circuit for this example is shown in Fig. 28, where we have included a parasitic capacitor C_1 in parallel with N_R . The real inductor is modeled by a series connection of an ideal linear inductor L and a linear resistance R_0 , as before.

Steady-State Solutions: Consider the case when R is 0 Ω ($G''_a < 0$). This circuit has a single unstable equilibrium point

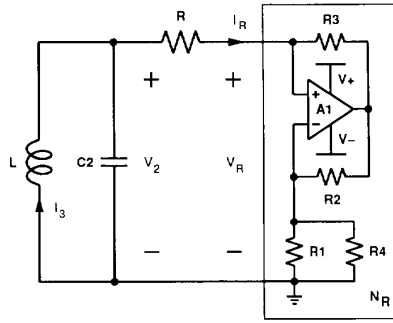


Fig. 27. Practical realization of the piecewise-linear circuit in Fig. 16. Components values are as in Fig. 13.

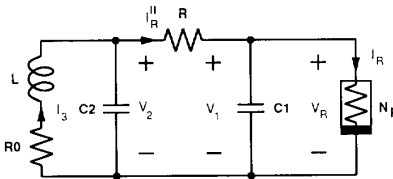


Fig. 28. Equivalent circuit for Fig. 27. R_0 models the series resistance of the inductor. C_1 is a parasitic transit capacitance.

$0''$ at the origin and is dissipative in its outer regions. The unique steady-state solution is a stable limit cycle.

Fig. 29(a) is an oscilloscope plot of the measured voltage waveform $V_1(t)$ for $R = 0\Omega$. The corresponding projection of the dynamics onto the V_1 - V_2 plane is shown in Fig. 29(b); compare this with Figs. 23 and 26.

Increasing R , the DP characteristic of the series combination of R and N_R develops a fold. As the characteristic passes through the I_3 axis, two new (stable) equilibria at P_+'' and P_-'' are born. The circuit then possesses three different steady-state solutions. Which one is observed experimentally depends on the initial conditions of I_{30} , V_{20} , and V_{10} .

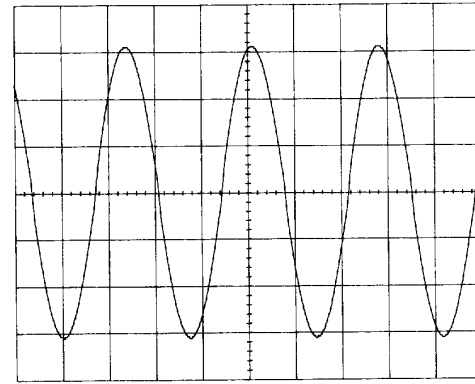
Equilibrium point: By short circuiting C_2 momentarily, one can force I_{30} , V_{20} , and V_{10} to the unstable equilibrium point at the origin from which the trajectory converges either to P_+'' or to P_-'' .

Fig. 30(a) is an oscilloscope plot of the measured dc voltage waveform $V_1(t)$ for $R = 2000\Omega$; this corresponds to the stable equilibrium point P_+'' .

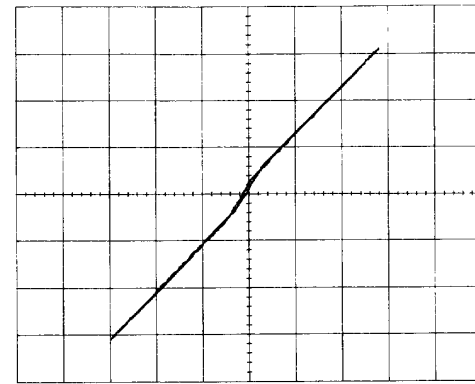
Limit cycle: These stable outer equilibrium points can be made to disappear by reducing R until the fold is smoothed out, and the circuit bursts into limit cycle oscillation once more. If P_-'' and P_+'' are then made to reappear by increasing R back to its initial value, the circuit remains in limit cycle behavior.

Fig. 30(a) is an oscilloscope plot of the measured voltage waveform $V_1(t)$ for $R = 2000\Omega$; this corresponds to the limit cycle shown in Fig. 24(b). The projection of the dynamics onto the V_1 - V_2 plane is shown in Fig. 30(c) and seems to exhibit "hysteresis" [19]; compare this with Figs. 24 and 26.

Note that the voltage waveform $V_1(t)$ is smooth when $G_a'' < 0$ and that it exhibits abrupt "jumps" once the fold appears ($G_a'' > 0$).



(a)



(b)

Fig. 29. Measured data for Fig. 27 with $R = 495\Omega$; the solution is a smooth limit cycle: (a) horizontal axis: time, $100\mu\text{s}/\text{div}$; vertical axis: $V_1(t)$, $1\text{ V}/\text{div}$; (b) projection of the limit cycle onto the V_2 - V_1 plane—horizontal axis: $V_1(t)$, $1\text{ V}/\text{div}$; vertical axis: $V_2(t)$, $1\text{ V}/\text{div}$.

6.3. Eigenvalues and Eigenvectors

Thus far, we have talked in general terms about the "fast" dynamics, "jumps" in the " V_1 direction," and evolution of the dynamics in the (I_3, V_2, V_1) coordinate system along planes defined by $G(V_2 - V_1) = f(V_1)$. Expressions for these directions, planes, and associated dynamics can be derived explicitly by studying the eigenvalues and eigenvectors of the Jacobian matrices in each region of the 3-D system (18)–(20).

Considering (20), we see that when C_1 is extremely small, V_1 changes rapidly ("jumps") until it satisfies $G(V_2 - V_1) - f(V_1) = 0$. Indeed, we can recover the original system (12)–(14) from Chua's circuit equations by setting $C_1 \equiv 0$. This is called a *singular perturbation* because it changes (20) from a differential equation to an algebraic equation.

We have the following result from the theory of singular perturbations:¹⁰ If either $(G + G_a) < 0$ or at least one of the eigenvalues of \mathbf{J}_{F_a}'' has a positive real part, then there exists C_1^* such that the equilibrium point at the origin of the 3-D circuit (18)–(20) is *unstable* for all $0 < C_1 < C_1^*$. Indeed, as $C_1 \rightarrow 0$, two eigenvalues (λ_+ and λ_-) of $0''$ approach those of \mathbf{J}_{F_a}'' , whereas the third (γ) approaches $-(G + G_a)/C_1$.

¹⁰This result follows from Theorem (37) on page 129 of [18].

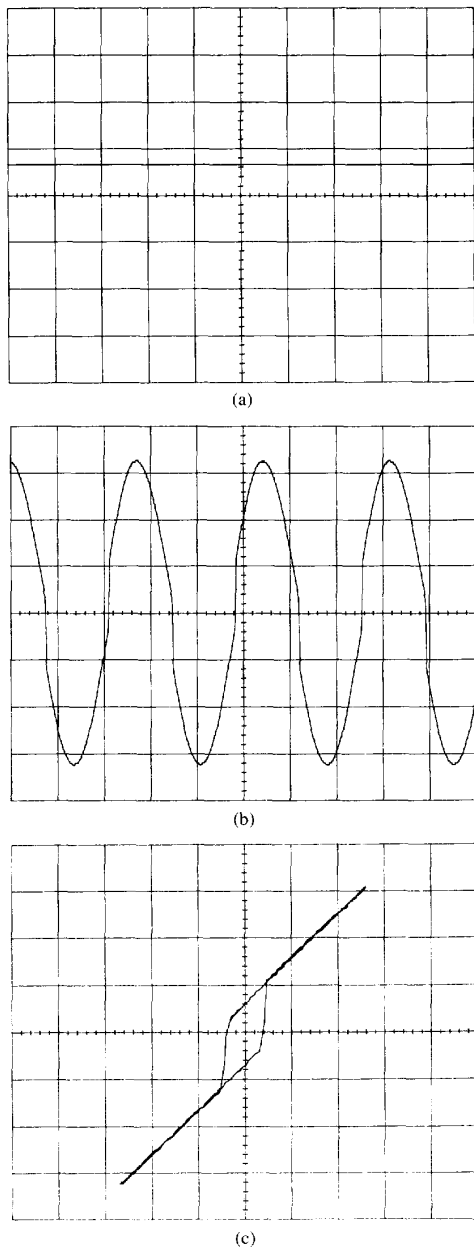


Fig. 30. Measured waveforms for Fig. 27 with $R = 2000\Omega$; the circuit has multiple steady-state solutions. (a) dc equilibrium point (P_+^*)—horizontal axis: time, $100\mu\text{s}/\text{div}$; vertical axis: $V_1(t)$, $1\text{V}/\text{div}$; (b) limit cycle enclosing all three equilibrium points—horizontal axis: time, $100\mu\text{s}/\text{div}$; vertical axis: $V_1(t)$, $1\text{V}/\text{div}$. Note that the voltage waveform $V_1(t)$ exhibits “jumps”; (c) projection of the limit cycle onto the V_2 - V_1 plane—horizontal axis: $V_2(t)$, $1\text{V}/\text{div}$; vertical axis: $V_1(t)$, $1\text{V}/\text{div}$.

As $C_1 \rightarrow 0$, the eigenvalue γ is the largest of the three in magnitude. The corresponding eigenvector aligns itself with the V_1 axis; we call this the “fast” eigenvector because it is associated with the largest eigenvalue. Furthermore, if $(G_a'')^2 < 4C_2/L$, λ_+ and λ_- are complex conjugates of the form $\sigma \pm j\omega$.¹¹ The real and imaginary parts of the

¹¹We denote $\sqrt{-1}$ by j .

corresponding eigenvectors span a plane in the (I_3, V_2, V_1) coordinate system, which is called a *complex eigenplane*. When $C_1 = 0$, this plane is defined by $G(V_2 - V_1) = G_a V_1$.

When $G_a'' > 0$, the real parts of the eigenvalues of $\mathbf{J}_{\mathbf{F}_a''}$ are negative. We concluded from our analysis of the reduced system (17) that the origin is a stable equilibrium point of the system. By definition, trajectories on the *complex eigenplane* remain indefinitely on that plane. Indeed, trajectories in the D_0'' region that lie on this stable eigenplane spiral toward the origin along the plane. However, any trajectory in D_1'' lying above or below the eigenplane will be repelled toward the outer regions by the fast parasitic dynamics along the eigenvector associated with γ .

By a similar analysis, it can be shown that (as long as $G_b'' > 0$) the outer equilibrium points are stable even when the parasitic dynamics are included.

We have seen that our 2-D D_0'' equivalent circuit has a *stable* equilibrium point at the origin when $G_a'' < 0$ if we neglect the parasitic transit capacitor C_1 . When we include an infinitesimal positive capacitance, the origin becomes *unstable*. Thus, although the origin of the singularly perturbed system (12)–(14) is *stable*, an arbitrarily small positive capacitance C_1 will render it *unstable*; failure to include this parasitic *completely* changes the stability properties of the origin. It is therefore *imperative* that the transit capacitance C_1 be included in parallel with N_R to complete the circuit model of Fig. 16. The resulting well-defined system of three ordinary differential equations describes Chua's circuit.

VII. CONCLUDING REMARKS

The 3-D continuous-time dynamical system (18)–(20) to which we have evolved in three steps from the parallel linear RLC circuit is simply Chua's circuit. We have seen that for a particular choice of parameters, this circuit can exhibit equilibrium point and limit cycle behavior. When can it exhibit chaos?

At this point, we invoke Shilnikov's theorem [13]. If the origin of our third-order autonomous circuit is an equilibrium point with a pair of stable complex eigenvalues $\sigma \pm j\omega$ ($\sigma < 0, \omega \neq 0$) and an unstable real eigenvalue γ satisfying $|\sigma| < \gamma$ and the vector field has a *homoclinic orbit*¹² through the origin, then the circuit can exhibit *horseshoes* [4] and chaos.

We have seen that when $C_1 \rightarrow 0$ and $(G_a'')^2 < 4C_2/L$, the origin of Chua's circuit has a stable pair of complex eigenvalues $\sigma \pm j\omega$ (the real and imaginary parts of whose eigenvectors span the plane $G(V_2 - V_1) = G_a V_1$) and an unstable real eigenvalue γ whose eigenvector points along the V_1 axis. For sufficiently small C_1 , $\gamma > |\sigma|$. This set of parameters satisfies all but one of the conditions for chaos in the sense of Shilnikov; the missing ingredient is a homoclinic orbit.

Chua realized that such an orbit could be produced by using unstable dynamics in the outer region of his circuit to

¹²A *homoclinic orbit* \mathcal{H} is the union of an equilibrium point \mathcal{E} and a trajectory \mathcal{T} that approaches \mathcal{E} asymptotically as $t \rightarrow \infty$ and as $t \rightarrow -\infty$ [4].

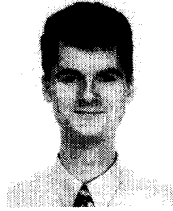
close a homoclinic trajectory onto itself; this requires that the slope G_b of the outer segments of the Chua diode N_R should be *negative*. In Part II of this paper, we study the chaotic dynamics of Chua's circuit when G_b is *negative*.

ACKNOWLEDGMENT

The author is grateful to Prof. L. Chua of UC Berkeley for his support and encouragement and to Prof. J. G. Lacy of University College Dublin for allowing the author to use his computer facilities.

REFERENCES

- [1] B. van der Pol and J. van der Mark, "Frequency demultiplication," *Nature*, vol. 120, no. 3019, pp. 363–364, Sept. 10, 1927.
- [2] M. P. Kennedy and L. O. Chua, "van der Pol and chaos," *IEEE Trans. Circuits Syst.*, vol. 33, no. 10, pp. 974–980, Oct. 1986.
- [3] H. G. Schuster, *Deterministic Chaos*. Weinheim, Germany: Physik-Verlag, 1984.
- [4] J. Guckenheimer and P. Holmes, *Nonlinear Oscillations, Dynamical Systems, and Bifurcations of Vector Fields*. New York: Springer-Verlag, 1983.
- [5] R. L. Devaney, *Chaotic Dynamical Systems*. Menlo Park, CA: Benjamin/Cummings, 1986.
- [6] L. O. Chua and T. Lin, "Chaos in digital filters," *IEEE Trans. Circuits Syst.*, vol. 35, no. 7, pp. 648–658, July 1988.
- [7] T. Endo and L. O. Chua, "Chaos from phase-locked loops," *IEEE Trans. Circuits Syst.*, vol. 35, no. 8, pp. 987–1003, Aug. 1988.
- [8] Y. S. Tang, A. I. Mees, and L. O. Chua, "Synchronization and chaos," *IEEE Trans. Circuits Syst.*, vol. CAS-30, no. 9, pp. 620–626, Sept. 1983.
- [9] A. Mees and L. O. Chua, "The Hopf bifurcation theorem and its application to nonlinear oscillation in circuits and systems," *IEEE Trans. Circuits Syst.*, vol. CAS-26, no. 4, pp. 235–254, Apr. 1979.
- [10] A. N. Willson, Jr., *Nonlinear Networks: Theory and Analysis*. New York: IEEE, 1975.
- [11] L. O. Chua, "Dynamic nonlinear networks: State of the art," *IEEE Trans. Circuits Syst.*, vol. CAS-27, no. 11, pp. 1059–1087, Nov. 1980.
- [12] ———, "Nonlinear circuits," *IEEE Trans. Circuits Syst.*, vol. CAS-31, no. 1, pp. 69–87, Jan. 1984.
- [13] L. O. Chua, M. Komuro, and T. Matsumoto, "The double scroll family, parts I and II," *IEEE Trans. Circuits Syst.*, vol. CAS-33, no. 11, pp. 1073–1118, 1986.
- [14] M. P. Kennedy, "Robust op amp realization of Chua's circuit," *Frequenz*, vol. 46, nos. 3–4, Mar.–Apr. 1992.
- [15] ———, "Experimental chaos via Chua's circuit," in *Proc. First Experimental Chaos Conf.*, 1992, pp. 340–351.
- [16] L. O. Chua, C. A. Desoer, and E. S. Kuh, *Linear and Nonlinear Circuits*. New York: McGraw-Hill, 1987.
- [17] M. W. Hirsch and S. Smale, *Differential Equations, Dynamical Systems, and Linear Algebra*. San Diego, CA: Academic, 1974.
- [18] M. Vidyasagar, *Nonlinear Systems Analysis*. Englewood Cliffs, NJ: Prentice-Hall, 1978.
- [19] M. P. Kennedy and L. O. Chua, "Hysteresis in electronic circuits: A circuit theorist's perspective," *Int. J. Circuit Theory Applications*, vol. 19, no. 5, pp. 471–515, 1991.
- [20] L. O. Chua and P. M. Lin, *Computer-Aided Analysis of Electronic Circuits: Algorithms and Computational Techniques*. Englewood Cliffs, NJ: Prentice-Hall, 1975.
- [21] L. O. Chua and A. -C. Deng, "Impasse points—Part I: Numerical aspects," *Int. J. Circuit Theory Applications*, vol. 17, pp. 213–235, 1989.
- [22] ———, "Impasse points—part II: Analytical aspects," *Int. J. Circuit Theory Applications*, vol. 17, pp. 271–282, 1989.



Michael Peter Kennedy was born in Dublin, Ireland, on April 25, 1963. He received the bachelor of engineering (electronics) degree with first class honors from University College Dublin (UCD) in 1984. He received the M.S. and Ph.D. degrees in electrical engineering from the University of California 1987 and 1991, respectively.

After receiving the Ph.D. degree, he worked as a Postdoctoral Research Fellow at the Electronics Research Laboratory, Berkeley, and as a visiting professor in the Chair of Circuits and Systems at the Ecole Polytechnique Fédérale de Lausanne, Switzerland. He returned to UCD in 1992 as a College Lecturer in the Department of Electrical and Electronic Engineering, where he teaches electronic circuits and computer-aided circuits and systems analysis. He also directs the undergraduate electronics laboratory. His current research interests are in simulation, design, analysis, synchronization, and control of nonlinear dynamical systems. His work on electronic instrumentation, computer-aided circuit analysis, neural networks, forced oscillators, piecewise-linear circuit theory, nonlinear dynamics, and signal processing has appeared in *Proceedings of the IEE*, *IEEE TRANSACTIONS ON CIRCUITS AND SYSTEMS*, *Artificial Neural Networks: Paradigms, Applications, and Hardware Implementations* (New York: IEEE), *International Journal of Circuit Theory and Applications*, *Frequenz*, and *Journal of Circuits, Systems, and Computers*.

Dr. Kennedy received UCD Scholarships from 1981–1983, the Best Bachelor's Thesis in Electronic Engineering Award in 1984, the National University of Ireland's Bursary in Electrical and Electronic Engineering in 1984, and the Scholarship Exchange Board Travelling Scholarship in 1985. While studying at the University of California at Berkeley, he was awarded a Semiconductor Research Corporation Scholarship and held the Wilson and Albert M. Flagg and Earle C. Anthony Scholarships. For his service to the international community at Berkeley, he received the International Volunteer Award. He received the 1991 Best Paper Award from the *International Journal of Circuit Theory and Applications* for his paper with L. Chua entitled "Hysteresis in Electronic Circuits: A Circuit Theorist's Perspective." In 1993, he was appointed Associate Editor of the *IEEE TRANSACTIONS ON CIRCUITS AND SYSTEMS—I: FUNDAMENTAL THEORY AND APPLICATIONS*.